PACS numbers: 42.55.Rz; 42.65.Ky; 42.60.By; 42.62.Fi
DOI: 10.1070/QE2001v031n06ABEH001987

A radiation source at 457 nm for high-resolution spectroscopy of a magnesium atom

S N Bagayev, V I Baraulya, A E Bonert, A N Goncharov, M P Seidaliev, S A Farnosov

***Abstract*. A ~ 20-mW cw radiation source is developed emitting at a wavelength of 457 nm with the linewidth less than 30 kHz. The source is based on a Ti:sapphire laser with frequency doubling in an external cavity containing a nonlinear LBO crystal. The results of high-resolution spectroscopy of magnesium atoms in separated optical fields, which demonstrate the possibilities of the system, are presented.**

Keywords: *Ti:sapphire laser, second-harmonic generation, high-resolution spectroscopy*.

1. Introduction

The energy level diagrams of alkali-earth elements Mg and Ca are of interest for the development of frequency standards in the visible [1–6] and microwave [7–10] spectral regions, as well as for the building of highly sensitive atomic interferometers for precision physical measurements [11].

To build an atomic interferometer based on magnesium atoms with the best possible parameters, a laser radiation source is required emitting at a wavelength of 457 nm with the linewidth of no more than 30 Hz and the output power ~ 50 mW. The precision spectroscopy of magnesium in the blue spectral region can be performed with the help of a dye laser pumped by a UV argon laser and actively frequency-stabilised relative to the transmission band of an external highly stable interferometer [1–3]. Another possibility of obtaining tunable radiation in the region of 457 nm is the use of frequency-doubled radiation from a Ti:sapphire laser at 914 nm.

The use of a Ti:sapphire laser offers a number of advantages. This solid-state laser is tunable in a very broad spectral range from 700 to 1100 nm, which allows one to obtain frequency-doubled radiation tunable from 350 to 550 nm. The Ti : sapphire laser is pumped by visible radiation from an argon laser, which is more reliable than a UV argon laser required for pumping a dye laser.

S N Bagayev, V I Baraulya, A E Bonert, A N Goncharov, M P Seidaliev, S A Farnosov Institute of Laser Physics, Siberian Division, Russian Academy of Sciences, prosp. akad. Lavrent'eva 13/3, 630090 Novosibirsk, Russia

Received 7 February 2001
Kvantovaya Elektronika **31** (6) 495–499 (2001)
Translated by M N Sapozhnikov

In contrast to a jet dye laser, the spectrum of perturbations of the frequency of a solid-state Ti:sapphire laser lies mainly in the frequency range up to 50 kHz, which substantially alleviates the problem of active stabilisation of the laser frequency. The use of a high-Q external cavity and efficient nonlinear crystals provides the generation of several hundreds of milliwatts of frequency-doubled radiation at the fundamental-frequency output of ~ 1 W.

In this paper, we report the development of a cw $Ti:Al_2O_3$ laser radiation source tunable in the region of 457 nm with the lasing linewidth less than 30 kHz and the output power ~ 20 mW.

2. Experimental

2.1 Ti:sapphire laser

A Ti:sapphire laser we used in our experiments was built on the basis of the optical scheme described in Ref. [12]. This scheme, optimised by us for lasing at 914 nm, is shown in Fig. 1.

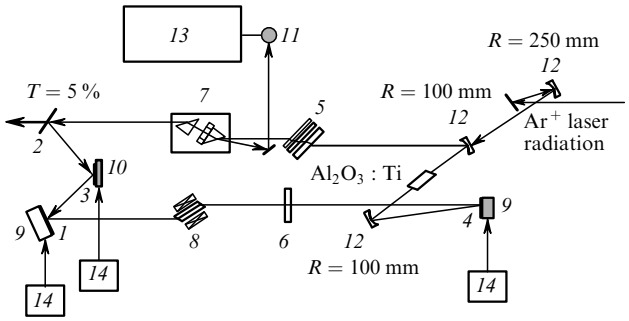

Figure 1. Optical scheme of a Ti:sapphire laser: (*1–4*) flat mirrors; (*5*) three-element Lyot filter; (*6*) etalon with a free spectral range (FRS) of 100 GHz; (*7*) etalon with a FSR of 20 GHz; (*8*) Faraday rotator; (*9*) 'slow' piezoelectric ceramics; (*10*) 'fast' piezoelectric ceramics; (*11*) photodiode; (*12*) spherical mirrors; (*13*) automatic selector control (ASC) system; (*14*) voltage supply for controlling piezoelectric mirrors.

Radiation from a pump argon laser was focused by a spherical mirror with the radius of curvature $R = 250$ mm into a $Ti:Al_2O_3$ crystal of length 15 mm through one of the mirrors ($R = 100$ mm) of the laser cavity. The ring cavity of the laser was formed by six mirrors: two spherical mirrors with $R = 100$ mm and four flat mirrors. The single-frequency generation and laser tuning to the required wave-

length were obtained with the help of a three-element Lyot filter and two etalons placed in the cavity. A thin etalon represented a plane-parallel quartz plate of thickness 1 mm without any coating. A thick etalon consisted of two Littrow prisms, which were separated by a 8-mm spacing, which can be changed with the help of piezoelectric ceramics. The inner surfaces of Littrow prisms had dielectric coatings with the reflectivity 30 %. The one-directional generation was provided by inserting an optical diode into the cavity. The optical diode consisted of a Faraday rotator and three mirrors, one of which (mirror *3*) was located outside the cavity plane. The Faraday rotator consisted of a Brewster rod of length 10 mm made of a MOS-31 magnetooptical glass and placed in the magnetic field of a permanent magnet ($Nd_{15}Fe_{77}B_8$). The Faraday rotator provided the optical rotation by $\sim 3^\circ$ at a wavelength of 914 nm.

To obtain the maximum width of the region of continuous laser tuning, which was limited only by dynamic characteristics of 'slow' piezoelectric ceramics, the thickness of the thick etalon was tuned to the cavity mode by the automatic selector control (ASC) system, which provided the laser action without mode jumps for a long time (~ 1 h). The laser frequency can be continuously tuned within 2 GHz. For the transmission coefficient of the output mirror $T = 5$ % and the pump power 18 W, the output power of the laser at 914 nm was 1 W.

The active stabilisation of the Ti:sapphire laser was provided by automatically tuning its frequency to the centre of the transmission band of an external highly stable Fabry–Perot interferometer. The scheme for the frequency stabilisation of the Ti:sapphire laser is shown in Fig. 2. The interferometer base represented a thick-walled Invar cylinder of length 500 mm and diameter 80 mm with an inner hole of diameter 18 mm. Mirrors with $R = 500$ mm were glued to the base ends. For the transmission coefficient of mirrors $T = 1$ %, the interferometer finesse F was ~ 300. A vacuum chamber, in which the interferometer was mounted with the help of vitone rings, was evacuated to a pressure of $10^{-4} - 10^{-5}$ Torr. A thermal stabilisation system provided the temperature stability of the interferometer base of the order of 10^{-3} °C.

The interferometer was tuned by applying voltage to the piezoelectric ceramics to which one of the interferometer mirrors was glued. The laser frequency was stabilised by the method of sidebands developed in Ref. [13]. Phase modulation at a frequency of 6 MHz was performed with an electrooptical modulator based on a lithium tantalate crystal $LiTaO_3$. The automatic frequency control (AFC) system consisting of two feedback circuits, a fast one and a slow one, provided the feedback bandwidth about of 30 kHz.

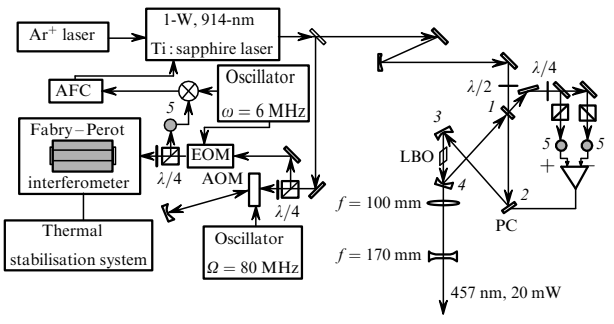

Figure 2. Optical scheme of a narrow-band radiation source emitting at 457 nm [(*1–4*) mirrors, (*5*) photodiodes].

Fig. 3 shows the spectrum of residual perturbations of the laser frequency observed using the AFC system. The laser linewidth $\Delta\nu$ in the stabilised regime was estimated to be ~ 15 kHz and was mainly limited by the stability of the Fabry–Perot interferometer itself, which was used for frequency stabilisation. We assume that the laser linewidth can be further decreased by improving the stability of the reference interferometer and increasing the bandwidth of the AFC system by using an intracavity electrooptical modulator.

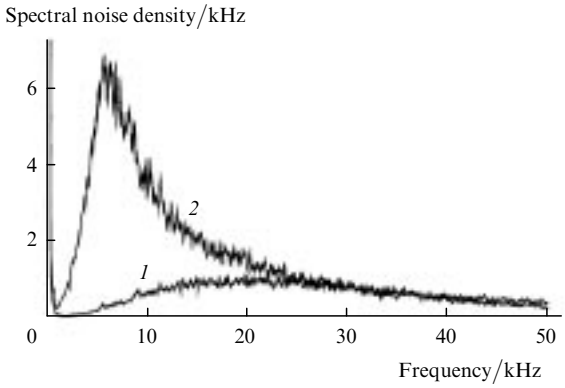

Figure 3. Spectral density of the perturbations of a Ti:sapphire laser frequency for the transmission band of an SK4-59 spectrum analyser equal to 100 Hz at maximum (*1*) and 10 times lower (*2*) gain in the negative feedback circuit.

2.2 SHG in an LBO crystal

The efficient SHG of radiation from a cw Ti:sapphire laser emitting at 914 nm can be produced in LBO, BBO, $LiIO_3$, and $KNbO_3$ crystals. The most promising among these crystals is a potassium niobate crystal $KNbO_3$ in which 90° noncritical phase matching is possible in this spectral region with the SHG efficiency exceeding 10^{-3} W^{-1}. However, this crystal was unavailable to us by the beginning of this study.

In accordance with a comparative analysis performed in paper [12], we have chosen a lithium triborate crystal LBO. This nonhygroscopic crystal provides the highest SHG efficiency at 914 nm among the crystals available to us. Its good optical quality and a relatively small birefringence angle (in our case, $\rho = 11$ mrad) provide sufficiently high spatial quality of radiation at 457 nm.

The SHG of 914-nm radiation occurs most efficiently when the radiation propagates in the XY plane of the crystal, with polarisation directed along the Z axis. With the angle φ between the wave vector $\boldsymbol{k}$ and the X axis equal to 23.8°, the phase matching condition is fulfilled for the first type conversion (ooe). For this conversion, the effective nonlinear coefficient is determined from the expression $d_{\text{eff}} = d_{32}\cos\varphi$, and for $d_{32} = (1.17 \pm 0.14) \times 10^{-12}$m V^{-1} [14], we have $d_{\text{eff}} = (1.07 \pm 0.13) \times 10^{-12}$ m V^{-1}. We calculated the SHG efficiency and the optimal focusing of radiation in the crystal using the results obtained in paper [15]. The SHG efficiency upon optimal focusing is

$$\gamma = \frac{P_{2\omega}}{P_\omega^2} = \frac{2\omega^2 d_{\text{eff}}^2 k_\omega L h_{\text{m}}}{\pi c^3 \varepsilon_0 n^3}\,\frac{1}{n}, \qquad (1)$$

where L is the crystal length; ω is the circular frequency of radiation; c is the velocity of light; ε_0 is the permittivity of vacuum; n is the refractive index of the crystal; and h_m is a dimensionless factor, which determines a decrease in the SHG efficiency due to a spatial separation of the first and second harmonics in the crystal. The factor $1/n$ in expression (1) is related to a decrease in the SHG efficiency when radiation is incident on the crystal at the Brewster angle due to a decrease in the radiation intensity in the crystal compared to the case of normal incidence. This decrease is caused by the beam expansion in the tangential plane [12]. With the birefringence parameter $B = \frac{1}{2}\rho(\omega nL/c)^{1/2} = 1.99$ and the crystal length $L = 1$ cm, the factor $h_m = 0.33$ and the optimal radius of the beam waist in the crystal $w_0 = 24$ μm. The calculated SHG efficiency $\gamma = (7 \pm 1.7) \times 10^{-5}$ W^{-1}.

We measured the SHG efficiency in a LBO crystal. The crystal geometry (3 mm × 3 mm × 10 mm) provided the incidence of radiation on its surface at the Brewster angle and its propagation inside the crystal at $\sim 23^\circ$ to the crystal axis in the XY plane. Radiation from the 400-mW Ti : sapphire laser was focused into the crystal by a lens with the focal length $f = 100$ mm. With such focusing, the beam waist radius in the crystal was nearly optimal. The radiation power at 457 nm was approximately 10 μW. The measured SHG efficiency equal to $\gamma_{ex} = (5.8 \pm 0.6) \times 10^{-5}$ W^{-1} is in good agreement with its calculated value.

To increase the radiation intensity at 457 nm, the nonlinear LBO crystal was placed inside an external ring cavity (see Fig. 2), which provided the 35-fold enhancement of the fundamental harmonic intensity in the crystal. In our case, the cavity quality was limited by losses at mirrors and crystal surfaces, which were estimated to be 2.7 % during the round trip in the cavity. The cavity, consisting of two flat (*1*, *2*) and two spherical (*3*), (*4*) mirrors with radii of curvature $R = 100$ mm, was designed for optimal ($w_0 = 24$ μm) focusing of radiation from the Ti:sapphire laser in the crystal. A total round-trip path in the cavity was 130 cm.

Radiation from the Ti:sapphire laser was coupled into the cavity through mirror (*1*) with $T = 3$ %. A Gaussian mode of the cavity was matched with the laser beam with the help of a spherical mirror with $R = 2$ m. The second harmonic radiation was outcoupled from the cavity through a dichroic mirror (*4*) with the transmission coefficient $T <$ 0.1 % at 914 nm and a high transmission coefficient $T \sim 90$ % at 457 nm. A spherical lens with $f = 100$ mm was used to collimate the second harmonic beam, and a cylindrical lens with the focal length $f = 170$ mm was used to correct for the beam astigmatism caused by the second-harmonic beam displacement in the LBO crystal.

The automatic cavity length control (ALC) system provided the coincidence of the centre of one of its transmission bands with the radiation frequency of the Ti:sapphire laser. The Hänsh – Couillaud polarisation method [16] was used for obtaining the error signal required for the operation of the ALC system. A small ($\sim 5^\circ$) angle between the polarisation plane of the input laser radiation and the cavity plane required for the polarisation method was produced with the help of a phase half-wave plate.

The dynamic characteristics of the ALC system provided the perturbation response band of ~ 30 kHz. Pulsations of the radiation power at 457 nm in the ALC regime did not exceed 5 %. For the 600-mW radiation power of the Ti : sapphire laser at the cavity input, the second-harmonic output power was 20 mW, in good agreement with the calculated value at the SHG efficiency $\gamma_{ex} = (5.8 \pm 0.6) \times 10^{-5}$ W^{-1} and intracavity losses equal to 2.7 %.

The radiation power at 457 nm can be increased by reducing intracavity losses. For example, a similar cavity described in paper [12] had losses equal to 0.7 %. In our case, this would mean more than a fivefold increase in the second-harmonic power. Unfortunately, mirrors with small losses that are required for this are not available to us. Another possibility of increasing the second-harmonic power is the use of a nonlinear $KNbO_3$ crystal, which is the most efficient in this spectral region.

2.3 Spectroscopy of the $^1S_0 - {}^3P_1$ intercombination transition in the Mg atom

The linewidth of our radiation source emitting at 457 nm is determined by the stability of the transmission band of the Fabry – Perot interferometer and by the accuracy of locking the Ti:sapphire laser frequency to this band. We estimated the interferometer stability based on the results of our previous paper [17], in which the stability of the transmission bands of interferometers was estimated to be 20 kHz from the beat signal of two Ar^+ lasers. The error of locking of the Ti:sapphire laser frequency to the transmission band of the interferometer was estimated from the error signal in the AFC feedback circuit and did not exceed 10 kHz. Taking these values into account, the laser emission linewidth was estimated as $\Delta\nu \leqslant 30$ kHz.

The most reliable information on the linewidth and the efficiency of the radiation source developed by us can be obtained in high-resolution spectroscopy experiments. We observed experimentally the Ramsey resonances in separated optical fields at the $^1S_0 - {}^3P_1$ transition in magnesium atoms. A simplified energy level diagram of the magnesium atom is presented in Fig. 4. A long lifetime of the upper $^3P_1$ level equal to 5.1 ms allows us to separate the optical fields by a great distance, which provides a high spectral resolution by observing resonances in these fields. Fig. 5 shows the scheme of the experiment on observing Ramsey resonances in separated laser fields.

A magnesium beam was formed by effusion of magnesium atoms from a source with a hole of diameter 0.8 mm into a vacuum chamber. The pressure of magnesium atoms in the source was determined by the temperature of its most

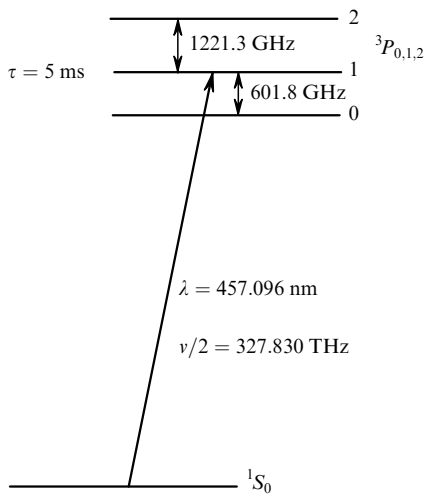

Figure 4. Energy level diagram of Mg.

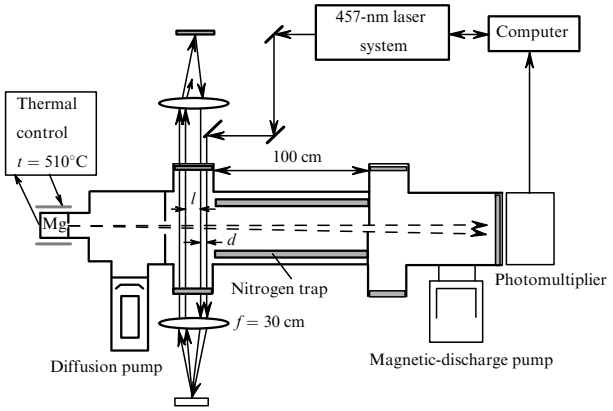

Figure 5. Scheme of the experiment for observation of Ramsey resonances in a magnesium atomic beam.

cold wall. The temperature was controlled by a thermocouple and was stabilised by the thermal stabilisation system. The operating temperature was 510°C, corresponding to the pressure of magnesium vapour of ~ 0.1 Torr. The distance from the beam source to the region of its interaction with the laser fields was ~ 50 cm. The atomic beam was collimated with a diaphragm of diameter 5 mm placed directly in front of the interaction region. The atomic density of the beam in the interaction region was estimated as 10^8 cm^{-3}, and the atomic flux through the region of interaction with laser fields was $\sim 10^{12}$ atom s^{-1}. The vacuum chamber was evacuated by diffusion and magnetic-discharge pumps down to the residual gas pressure of $\sim 10^{-6}$ Torr.

The laser radiation was injected into the vacuum chamber through plane–parallel quartz windows with antireflection coatings. The required configuration of four parallel laser beams was produced with the help of the optical system consisting of two 'cat's eye' type reflectors. Each reflector consisting of a two-lens objective with $f = 30$ cm and a flat mirror located at its focus was preliminary adjusted. After the adjustment, the laser beams were parallel to each other with an error of $\sim 10^{-5}$ rad.

The optical system was aligned so that the optical axes of the reflectors were parallel to each other and perpendicular to the atomic beam. By changing the distance between the optical axes of the reflectors and the position of the input laser beam, we could vary both the distance l between pairs of copropagating laser beams and the distance d between the laser beams in a pair. In our experiment, the distance l was determined by the aperture of the optical windows of the vacuum chamber and was equal to 3 cm. The distance d, which determined the width of Ramsey resonances, was taken to be ~ 3 mm. In this case, the width of Ramsey resonances should be ~ 30 kHz. Diameters of the laser beams in the interaction region were $2w_0 \sim 1$ mm for the radiation power ~ 5 mW.

We detected the luminescence signal from a magnesium beam induced by laser fields. This signal is proportional to the population of the upper $^3P_1$ level. Because the lifetime of the $^3P_1$ level is $\tau = 5.1 \times 10^{-3}$ s, we could detect the luminescence signal at a large distance from the interaction region. The luminescence signal from the beam decreases by a factor of 2.7 at a distance of $\langle v\rangle\tau \approx 4$ m ($\langle v\rangle$ is the velocity of atoms in the beam).

We detected the luminescence signal from the excited magnesium beam with a photomultiplier at a distance of ~ 1 m from the interaction region. Our system for collecting the luminescence signal provided the detection of $\sim 1/100$ part of luminescence photons with the quantum yield $\eta \sim 0.15$. The separation of the regions of excitation and detection resulted in a substantial decrease in the background stray laser radiation, thereby increasing the signal-to-noise ratio.

Fig. 6 shows the first derivative of the absorption line profile at the $^1S_0 - {}^3P_1$ transition in separated optical fields. The signal was recorded by modulating the radiation frequency at the modulation frequency $f_m = 182$ Hz with the amplitude of 30 kHz. The output signal from the photomultiplier was detected with a lock-in anplifier. The output signal from the lock-in anplifier was recorded as a function of the laser frequency detuning.

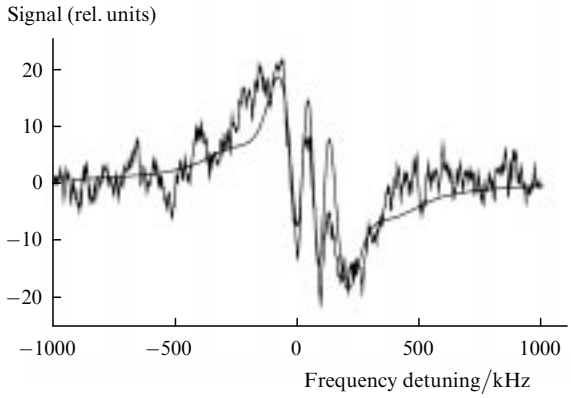

Figure 6. Absorption line shape observed upon the interaction of the 457-nm radiation with an atomic beam in the geometry of four separated fields for the integration constant of a lock-in amplifier $\tau = 3$ s, and the calculated line shape (the solid curve without noise).

We analysed the experimental results using the qualitative theory of the interaction of four separated fields with an atomic beam. The luminescence signal detected in our experiments is proportional to the population of the $^3P_1$ level after the interaction of a magnesium atomic beam with the optical fields. The upper level population is determined by the expression

$$N \propto \int_{v_\perp=0}^{\infty}\int_{v_{||}=-\infty}^{\infty} F(v_\perp, v_{||})\left\{A_\pm\left(\frac{\Delta w_0}{v_\perp}\right)\right.$$

$$\left.\times\cos\left[\frac{(\Delta \pm \delta)2d}{v_\perp} + \varphi_L\right] + A_{nc}(\Delta)\right\} dv_\perp dv_{||}, \qquad (2)$$

where $\Delta = \omega - \omega_0$ is the radiation frequency detuning relative to the unperturbed transition; $\delta = \hbar k^2/2m \approx 2\pi(40 \times 10^3)$ s^{-1} is the recoil frequency; k is the wave number; $F(v_\perp, v_{||})$ is the velocity distribution function of atoms in the beam in the transverse and longitudinal directions with respect to the laser beam propagation; w_0 is the waist of the laser beam; $A_\pm(\Delta w_0/v_\perp)$ is the envelope function with the characteristic width equal to the inverse time of flying of atoms through the laser beam; $\varphi_L = \varphi_2 - \varphi_1 + \varphi_4 - \varphi_3$ is the phase term that determines the relative phases of the four laser fields; and $A_{nc}(\Delta)$ is the function describing the incoherent part of the interaction of radiation with the atomic beam.

After integration over the velocity distribution of atoms in the beam, the incoherent part describes the line profile with the width equal to the residual Doppler broadening $k\langle v\rangle\theta$ (where θ is the divergence angle of the atomic beam). A dip in the centre of this profile has a characteristic width, which is equal to the inverse time of flying of atoms through the laser beam $\sim\langle v\rangle/w_0$. In the case of an effusion beam with a broad velocity distribution, the coherent part of the interaction describes two profiles with characteristics widths equal to half the inverse time of flying of atoms between the fields in a pair of copropagating laser fields $\langle v\rangle/2d$. These two profiles correspond to the recoil doublet.

Expression (2) describes the signal shape only qualitatively by neglecting relaxation during flying of atoms through the region of interaction with light fields. The signal shape can be calculated exactly using the theory developed in paper [18].

The solid curve in Fig. 6 shows the first derivative of the absorption line shape calculated by expression (2) with the experimental values of the parameters d and w_0, and the probe modulation of the laser frequency equal to 30 kHz. The experimental line shape coincides qualitatively with the calculated shape. In the experiment, the recoil doublet with the splitting between components equal to 80 kHz was resolved. Comparison of the experimental line shape with the calculated one suggests that the resolution of our laser spectrometer is no worse than 30 kHz, and, hence, the laser linewidth at 457 nm is $\Delta\nu \leqslant 30$ kHz.

3. Conclusions

We have built a narrow-band radiation source tunable in the region of 457 nm for spectroscopy of the magnesium atom. The source is based on a Ti:sapphire laser with frequency doubling in an external cavity containing a nonlinear LBO crystal. The linewidth of the ~ 20-mW source is $\Delta\nu \leqslant 30$ kHz. The experimental observation of Ramsey resonances in separated optical fields with the resolution ~ 30 kHz have demonstrated that this source can be used for high-resolution spectroscopy of the magnesium atom. The output power of the source can be considerably increased by using a more efficient nonlinear potassium niobate crystal $KNbO_3$. To reduce the emission linewidth $\Delta\nu$ below 1 kHz, we plan to use a new highly stable Fabry–Perot interferometer with the finesse $F \sim 10^4$ made of a zerodur with high-quality mirrors and a fast frequency stabilisation system with the operating band broader than 300 kHz based on an intracavity phase electrooptical modulator.

Note that upon pumping a Ti : sapphire laser by a high-power 532-nm cw Nd:YVO_4/LBO laser, our system will represent an all-solid-state laser system. The possibility of using this system for obtaining narrow-band cw radiation tunable from 0.7 to 1.1 μm and from 0.35 to 0.55 μm upon frequency doubling in nonlinear crystals makes this system a unique tool for high-resolution spectroscopy of atoms and molecules.

Acknowledgements. The authors thank A M Yurkin, N A Pyl'neva, I A Lisova ('Siberian Single Crystal–EKSMA) for synthesis of LBO crystals. This work was supported by the Russian Foundation for Basic Research (Grants Nos 96-02-05854 and 99-02-17141).

References

1. Sterr U, Sengstok K, Muller J H, Bettermann D, Ertmer W *Appl. Phys. B* **54** 341 (1992)
2. Sterr U, Sengstok K, Muller J H, Bettermann D, Ertmer W *Appl. Phys. B* **56** 62 (1993)
3. Sengstok K, Sterr U, Muller J H, Rieger V, Bettermann D, Ertmer W *Appl. Phys. B* **59** 99 (1994)
4. Morinaga A, Riehle F, et al. *Appl. Phys. B* **48** 165 (1989)
5. Morinaga A, Riehle F, Ishikawa J, Helmcke J *IEEE Trans. Instrum. Meas.* **38** 524 (1989)
6. Ito N, Ishikawa J, Morinaga A *J. Opt. Soc. Am. B: Opt. Phys.* **8** 1388 (1991)
7. Strumina F *Metriologia* **8** 85 (1972)
8. Godone A, Bava E, Giusfredi G, Novero C, Wang Yu-Zhu *Opt. Commun.* **59** 263 (1986)
9. Beverini N, De Pascalis S, Maccionni E, Pereira D, Strumina F, Vissani G, Wang Y Z, Novero C *Opt. Lett.* **14** 350 (1989)
10. Godone A, Novero C *Metrologia* **30** 163 (1993)
11. Sterr U, Sengstok K, Ertmer W, Riehle F, Helmcke J In: *Atom Inteferometry* (San Diego: Academic Press, 1997), p. 293
12. Bourzeix S, Plimmer M D, et al. *Opt. Commun.* **99** 89 (1993)
13. Drever R W P, Hall J L, Kowalski F W, Hough J, Ford G M, Munley A J, Ward H *Appl. Phys. B* **31** 97 (1983)
14. Data provided by the LBO crystal manufacturer 'Siberian Single Crystal – Eksma'
15. Boyd G D, Kleinman D A *J Appl. Phys.* **39** 3597 (1968)
16. Hänsch W, Couillaud B *Opt. Commun.* **35** 441 (1980)
17. Chebotayev V P, Goldort V G, Goncharov A N, Ohm A E, Skvortsov M N *Metrologia* **27** 61 (1990)
18. Borde' Ch J, Salomon Ch, Avriller S, van Lerberghe A, Breant Ch, Bassi D, Scoles G *Phys. Rev. A* **30** 1836 (1984)